Theory of electronic and optical properties of magnetoexcitons in quantum-well wires

M. Graf and P. Vogl
Walter Schottky Institut and Physik Department, TU München, 85748 Garching, Germany

A. B. Dzyubenko
General Physics Institute, Russian Academy of Sciences, Moscow 117942, Russia
(Received 22 February 1996; revised manuscript received 7 August 1996)

Binding energies and linear optical properties of quasi-one-dimensional excitons in a quantum wire in strong magnetic fields are predicted. It is shown that magnetoexcitons confined in a quantum-well wire possess a hydrogenic spectrum with bound states and a continuum of scattering states, in contrast to two-dimensional magnetoexcitons that are always bound. The appearance and shape of Fano resonances in the optical spectra are explained and the influence of the Coulomb interaction on the optical spectra is discussed both analytically and numerically. [S0163-1829(96)00547-4]

I. INTRODUCTION

The Coulomb interaction between electrons and holes in a semiconductor subject to a strong quantizing magnetic field leads to the formation of magnetoexcitons. In bulk semiconductors, their properties are well understood.[1–3] There are both bound as well as unbound excitonic states. The former appear energetically below each free electron and hole Landau level pair. Those associated with higher Landau levels interact with the unbound states associated with the lower Landau levels and form Fano resonances.[4] These resonances show up in the optical absorption spectrum and have been studied theoretically and experimentally.[5,6]

In two dimensions (2D) with a magnetic field perpendicular to the plane, all magnetoexciton states are bound even though their spectrum consists of energy bands of finite width.[7–10] The finite dispersion is a consequence of the Coulomb interaction. Since only zero momentum transitions are optically allowed, the absorption spectrum consists solely of discrete transitions.[11] For one-dimensional (1D) systems such as quantum wires, one might expect an even more pronounced localization of magnetoexcitons and, correspondingly, a strictly discrete optical spectrum. On the other hand, the spectrum of independent particles in a quantum wire subject to a magnetic field is known to form a continuum.[12] So far, only the ground-state energy of 1D magnetoexcitons has been studied[12–14] but not their optical absorption spectrum.

In this paper, we present a systematic study of the electronic and optical properties of the ground and excited states of laterally confined 2D magnetoexcitons and show the spectrum of 1D magnetoexcitons to contain both discrete bound states as well as a continuum of unbound states, in contrast to the 2D case. Thus, we find that 1D magnetoexcitons resemble more closely the 3D situation, whereas zero-dimensional magnetoexcitons[15,16] only show discrete optical transitions again, analogously to the situation in two dimensions. In spite of their similarity, we also find marked differences between 1D and 3D magnetoexcitons. In the 1D case, there are Fano resonances in the optical absorption spectrum that are associated with optically forbidden quasibound states. In addition, the Coulomb interaction smooths the absorption edge of unbound magnetoexcitons, which exhibits an inverse square-root singularity for independent particles.[17]

In the absence of magnetic fields, optical properties of 1D excitons[18,19] and the interaction between bound and scattering states[20] has been investigated before. Here, we generalize these results to high magnetic fields and provide a qualitative explanation of the characteristic features of the magnetoexciton absorption spectrum.

The paper is structured as follows. In Sec. II, we express the Schrödinger equation for 1D magnetoexcitons in the basis of 2D magnetoexcitons, assuming a parabolic confinement potential for electrons and holes. In Sec. III, we calculate the optical absorption spectrum of magnetoexcitons in GaAs wires of several widths. A discussion of the results follows in Sec. IV. We show that all prominent features in the optical spectra can be identified and explained in terms of approximate solutions for 1D excitons that neglect the coupling between different Landau levels. Finally, we conclude in Sec. V and provide a brief derivation of the magnetoexciton Coulomb matrix elements in the Appendix.

II. EQUATIONS OF MOTION FOR CONFINED MAGNETOEXCITONS

In this section, we study the two-particle Schrödinger equation of two-dimensional electrons and holes with Coulomb attraction in a strong magnetic field and a confining parabolic wire-type potential. We express this Schrödinger equation in the basis of two-dimensional magnetoexcitons and provide analytical expressions for the Coulomb matrix elements therein. A parabolic two-band model is employed for electrons and holes throughout this paper. We take the two-dimensional plane of the electron gas to be the $x_\perp - x_\parallel$ plane and assume a magnetic field B perpendicular to this plane. In addition, we allow for one-particle potentials in the $x_\perp$ direction that represent the confinement to a quasi-one-dimensional system along the remaining $x_\parallel$ direction (see Fig. 1). The Hamiltonian reads, in units of $\hbar = 1$,

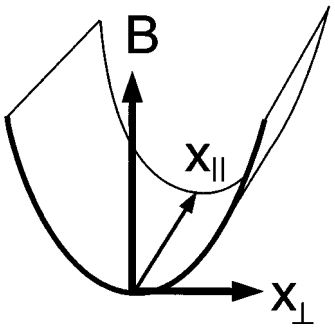

FIG. 1. Schematic view of the geometry used in this paper. The confinement in $x_\perp$ direction generates a quantum wire along the $x_\parallel$ direction. The exciton is subjected to a perpendicular magnetic field B.

$$\hat{H}=\hat{H}_0+\hat{V}_e+\hat{V}_h$$
$$=\frac{1}{2m_e}\left(\mathbf{p}_e+\frac{e}{c}\mathbf{A}_e\right)^2+\frac{1}{2m_h}\left(\mathbf{p}_h-\frac{e}{c}\mathbf{A}_h\right)^2$$
$$+U_{e-h}(\mathbf{r}_e-\mathbf{r}_h)+V_e(x_\perp^e)+V_h(x_\perp^h). \quad (1)$$

Here, $U_{e\text{-}h}$ denotes the Coulombic electron-hole interaction, and V_e and V_h are the external potentials that confine the electrons (e) and holes (h), respectively. Their respective effective masses are denoted by m_e and m_h.

The confinement of a three-dimensional electron gas to two dimensions increases the minimum energy gap. The zero of energy in Eq. (1) is taken to be this effective two-dimensional energy gap and is denoted by E_{gap}. Additionally, the confinement splits the valence band edge states into subbands. Within the four-band Luttinger band model,[21,22] the uppermost hole subband is characterized by the in-plane effective mass of $m_h=1/(\gamma_1+\gamma_2)$, where γ_1 and γ_2 are the bulk Luttinger parameters. In our numerical calculations, we have used this mass rather than the bulk hole mass.

Since the single-particle potentials provide a barrier for the carriers in the $x_\perp$ direction, it is practical to use the Landau gauge $\mathbf{A}=B(0,x_\perp,0)$. In the regime of strong magnetic fields, the most suitable basis for Eq. (1) is a product of electron and hole Landau states with quantum numbers n and m $(n,m=0,1,\ldots)$, respectively,

$$\phi^e_{n,k_\parallel}(\mathbf{r}_e)=\frac{1}{\sqrt{2\pi\ell}}e^{ik_\parallel x^e_\parallel}\chi_n(x^e_\perp/\ell+k_\parallel\ell),$$

$$\phi^h_{m,k_\parallel}(\mathbf{r}_h)=\frac{1}{\sqrt{2\pi\ell}}e^{ik_\parallel x^h_\parallel}\chi_m(x^h_\perp/\ell-k_\parallel\ell). \quad (2)$$

The functions χ_n are one-dimensional harmonic oscillator eigenfunctions with corresponding single-particle energies $\epsilon^p_n=\omega_p\ (n+1/2)=(eB/m_pc)\ (n+1/2)$, and $\ell=(c/eB)^{1/2}$ is the magnetic length. In order to simplify the notation, single-particle quantities are labeled throughout by a common index p that stands for electrons and holes.

These equations show the dual role of the electron or hole variable $k_\parallel$ that is characteristic for particles in a magnetic field. The variable $k_\parallel$ acts as a momentum for the motion in the $x_\parallel$ direction, whereas $k_\parallel\ell^2$ is the spatial center coordinate for the motion in $x_\perp$ direction. To maintain physically transparent expressions, we therefore keep the magnetic length explicitly in our equations.

Since the total one-dimensional exciton momentum $K_\parallel=k^e_\parallel+k^h_\parallel$ is conserved for confining potentials $V_p(x_\perp)$, in contrast to the exciton momentum $K_\perp$ in $x_\perp$ direction, we can expand the eigenstates of the Hamiltonian $\hat{H}$ into the basis functions[23,24] $\psi_{nmK_\perp}(\mathbf{r}_e,\mathbf{r}_h)$, representing two-dimensional magnetoexcitons with given magnetic center-of-mass momentum $\mathbf{K}=(K_\perp,K_\parallel)$. Since we concentrate on the optical absorption spectrum in this paper, only magnetoexcitons with $K_\parallel=0$ need to be considered. These eigenstates can be expressed by

$$\Psi(\mathbf{r}_e,\mathbf{r}_h)=\sum_{n,m}\int dK_\perp\ \ \Phi_{nm}(K_\perp)\ \ \psi_{nmK_\perp}(\mathbf{r}_e,\mathbf{r}_h), \quad (3)$$

$$\psi_{nmK_\perp}(\mathbf{r}_e,\mathbf{r}_h)$$
$$=\frac{1}{\sqrt{2\pi}}\int dk_\parallel\ \ e^{iK_\perp k_\parallel\ell^2}\ \ \phi^e_{n,-k_\parallel}(\mathbf{r}_e)\ \ \phi^h_{m,k_\parallel}(\mathbf{r}_h), \quad (4)$$

with expansion coefficients $\Phi_{nm}(K_\perp)$.

In this basis, the Schrödinger equation with eigenvalue E reads

$$\sum_{n'}\frac{1}{\sqrt{2\pi}}\int dq\ s_{n,n'}(q)\ \ V_e(q)\ \ \Phi_{n'm}(K_\perp-q)$$
$$+\sum_{m'}\frac{1}{\sqrt{2\pi}}\int dq\ s_{m,m'}(q)\ \ V_h(q)\ \ \Phi_{nm'}(K_\perp-q)$$
$$+\sum_{n',m'}\frac{e^2}{2\ell\epsilon}U_{nm,n'm'}(K_\perp\ell)\ \ \Phi_{n'm'}(K_\perp)$$
$$=(E-\epsilon^e_n-\epsilon^h_m)\Phi_{nm}(K_\perp), \quad (5)$$

where ϵ is the dielectric constant and the functions

$$s_{n,n'}(q)=\langle\chi_n|\exp(iqx_\perp)|\chi'_n\rangle \quad (6)$$

can easily be evaluated in terms of the generalized Laguerre polynomials. The functions $V_p(q)$ are the Fourier transforms of the one-dimensional potentials $V_p(x_\perp)$. The dimensionless matrix elements $U_{nm,n'm'}$ represent the e-h interaction in the basis of Eq. (4),

$$U_{n'm',nm}(K_\perp\ell)=-2\int\int d\mathbf{r}_e\ \ d\mathbf{r}_h\ \ \psi^*_{n'm'K_\perp}(\mathbf{r}_e,\mathbf{r}_h)$$
$$\times\frac{\ell}{|\mathbf{r}_e-\mathbf{r}_h|}\ \ \psi_{nmK_\perp}(\mathbf{r}_e,\mathbf{r}_h). \quad (7)$$

We show in the Appendix that these matrix elements can be cast into the following analytic form:

$$U_{n'm',nm}(K_\perp\ell)=-\left(\frac{i\ K_\perp\ell}{\sqrt{2}}\right)^N\sum_{L=0}^{n+m'}B^{(L)}_{n'm',nm}\frac{\Gamma(N+L+\frac{1}{2})}{\Gamma(N+1)}\ {}_1F_1\left(N+\tfrac{1}{2}+L;\ N+1;\ -\frac{(K_\perp\ell)^2}{2}\right),$$

$$B^{(L)}_{n',m';n,m}=\frac{(-1)^{n'-n+L}}{L!}\sqrt{2\ \frac{n!\ m'!}{n'!\ m!}}\sum_{l=0}^{n}\binom{n'}{n-l}\binom{m}{m'-L+l}\binom{L}{l},\tag{8}$$

where $N=n'-n-m'+m$ and ${}_1F_1$ is the degenerate hypergeometric function.[25] For a few special cases, analytic expressions of the Coulomb matrix elements have already been obtained previously.[7,9,26] One can easily verify that the general expression Eq. (8) and the definition $\kappa^2=K_\perp^2\ell^2/4$ yield

$$U_{00,00}(K_\perp\ell)=-\sqrt{2\pi}\ e^{-\kappa^2}\ I_0(\kappa^2),$$

$$U_{10,10}(K_\perp\ell)=-\sqrt{2\pi}\ e^{-\kappa^2}\left[\left(\frac{1}{2}+\kappa^2\right)\ I_0(\kappa^2)-\kappa^2\ I_1(\kappa^2)\right],\tag{9}$$

$$U_{11,11}(K_\perp\ell)=-\sqrt{2\pi}\ e^{-\kappa^2}\left[\left(\frac{3}{4}-\kappa^2+2\kappa^4\right)\ I_0(\kappa^2)-2\kappa^4\ I_1(\kappa^2)\right],$$

in accord with previous results.[7] In this equation, the functions I_ν are the modified Bessel functions.

We write the confining parabolic potentials for electrons and holes ($p=e,h$) in the form of

$$V_p(x_\perp)=m_p\Omega_p^2x_\perp^2/2,\tag{10}$$

where the frequency Ω_p is related to the width parameter $L_p=1/\sqrt{m_p\ \Omega_p}$. Since the Fourier transform of such a potential reads

$$V_p(k)=-\sqrt{\pi/2}\ m_p\Omega_p^2\delta''(k),\tag{11}$$

the integral equation (5) becomes a system of ordinary differential equations. It is useful to define a weighted average Ω of the frequencies Ω_p and a parameter s that measures the difference in confinement of electrons and holes,

$$\mu\ \Omega^2=m_e\ \Omega_e^2+m_h\ \Omega_h^2,$$

$$s=\frac{m_e\ \Omega_e^2-m_h\ \Omega_h^2}{\mu\ \Omega^2},\tag{12}$$

where μ is the reduced electron-hole mass ($\mu^{-1}=m_e^{-1}+m_h^{-1}$). By inserting Eq. (11) into Eq. (5) we obtain the set of coupled differential equations,

$$\begin{aligned}
&-\frac{1}{2\mu_{\rm eff}}\frac{d^2\Phi_{n\,m}(K_\perp)}{d(K_\perp\ell^2)^2}+i\frac{1+s}{4\mu_{\rm eff}\ell}\left(\sqrt{\frac{n}{2}}\frac{d\Phi_{n-1\,m}(K_\perp)}{d(K_\perp\ell^2)}+\sqrt{\frac{n+1}{2}}\frac{d\Phi_{n+1\,m}(K_\perp)}{d(K_\perp\ell^2)}\right)+i\frac{1-s}{4\mu_{\rm eff}\ell}\left(\sqrt{\frac{m}{2}}\frac{d\Phi_{n\,m-1}(K_\perp)}{d(K_\perp\ell^2)}\right.\\
&\left.+\sqrt{\frac{m+1}{2}}\frac{d\Phi_{n\,m+1}(K_\perp)}{d(K_\perp\ell^2)}\right)+\frac{1+s}{8\mu_{\rm eff}\ell^2}[\sqrt{n\ \ (n-1)}\ \ \Phi_{n-2\,m}(K_\perp)+\sqrt{(n+2)\ \ (n+1)}\ \ \Phi_{n+2\,m}(K_\perp)]\\
&+\frac{1-s}{8\mu_{\rm eff}\ell^2}[\sqrt{m\ \ (m-1)}\ \ \Phi_{n\,m-2}(K_\perp)+\sqrt{(m+2)\ \ (m+1)}\ \ \Phi_{n\,m+2}(K_\perp)]\\
&+\sum_{n',m'}\frac{e^2}{2\ell\epsilon}U_{nm,n'm'}(K_\perp\ell)\ \ \Phi_{n'\ m'}(K_\perp)=(E-I_{n\,m})\Phi_{n\,m}(K_\perp),
\end{aligned}\tag{13}$$

where all constant terms have been lumped together and are given by

$$I_{nm}=\left(\omega_e+\frac{\Omega_e^2}{2\omega_e}\right)\left(n+\frac{1}{2}\right)+\left(\omega_h+\frac{\Omega_h^2}{2\omega_h}\right)\left(m+\frac{1}{2}\right).\tag{14}$$

In these equations, the parameter $\mu_{\rm eff}=\mu\omega_c^2/\Omega^2$ plays the role of an effective mass, where $\omega_c=eB/\mu c$ is the cyclotron frequency. The states represented by the different Landau level pairs (n,m) may be termed ''channels'' with the channel wave functions $\Phi_{nm}(K_\perp)$. The kinetic energy term and the diagonal part of the potential U describes the motion within the individual channels. The other terms couple the channels with one another. The terms originating from the parabolic confinement couple each channel (n,m) only to its neighboring channels, whereas the Coulomb term $U_{nm,n'm'}$ couples all channels with one another.

Equation (13) may be written in a compact matrix form as

$$\left(-\boldsymbol{A}\frac{d^2}{d(K_\perp\ell^2)^2}-i\ \ \boldsymbol{B}\frac{d}{d(K_\perp\ell^2)}+\boldsymbol{C}(K_\perp)-E\ \ \mathbf{1}\right)\boldsymbol{\Phi}(K_\perp)=\mathbf{0}.\tag{15}$$

Equation (15) may be considered as a multichannel scattering problem. If there is no Coulomb interaction, the solutions $\mathbf{\Phi}$ are known to form a continuum of propagating states.[17] The Coulomb interaction has two effects: first, it modifies this continuum and, secondly, it introduces bound states. In order to be able to accurately resolve the induced resonances in the continuum as well as to calculate the bound states, we employ a scattering approach.

First, we note that the Coulomb matrix elements vanish for large $|K_\perp|$. As a consequence, Eq. (15) becomes translationally invariant in $K_\perp$ in this limit. For given energy E, its asymptotic solutions are propagating or evanescent wave functions,

$$\mathbf{\Phi}^\lambda(K_\perp) \xrightarrow{|K_\perp|\to\infty} \boldsymbol{c}^\lambda \frac{\ell}{\sqrt{2\pi}} \exp(iK_\perp \ell^2 \lambda). \tag{16}$$

This expression neglects the Coulomb phases since they have a negligible influence on the optical properties that we focus on in this work. The vector $\boldsymbol{c}^\lambda$ and the (complex) wave number λ are determined by the quadratic eigenvalue equation in λ that follows from inserting Eq. (16) into Eq. (15) and setting the Coulomb matrix elements equal to zero. This gives

$$[\lambda^2 \ \boldsymbol{A}+\lambda \ \boldsymbol{B}+\boldsymbol{C}(\infty)-E \ \mathbf{1}]\boldsymbol{c}^\lambda = \mathbf{0}, \tag{17}$$

where $\boldsymbol{C}(\infty)=\boldsymbol{C}(K_\perp\to\infty)$. Such a quadratic eigenvalue problem can be transformed into a linear one and solved by standard techniques.[27] Naturally, only a finite number of Landau level pairs (n,m) are taken into account in the actual numerical solution of Eq. (17). This is justified for sufficiently high magnetic fields, $\ell < L_p$.

As a result, one obtains a finite number of eigenvalues λ_i and the corresponding asymptotic solutions $\boldsymbol{c}^{\lambda_i}$ for given energy E. The solutions with real eigenvalues λ_i represent the confined wire states of independent electrons and holes.[17] Accordingly, real eigenvalues are found only for energies larger than the zero-point energy $I_0=(\sqrt{\omega_e^2+\Omega_e^2}+\sqrt{\omega_h^2+\Omega_h^2})/2$. We also note that a normalization of the eigenvectors $\boldsymbol{c}^{\lambda_i}$ to unity ensures a δ normalization of the propagating asymptotic wave functions (16), $\int \mathbf{\Phi}^{\lambda_i *}\mathbf{\Phi}^{\lambda_j} dK_\perp = \delta(\lambda_i-\lambda_j)$.

Once we have determined all asymptotic solutions for the given energy E, we can determine the linear combination that corresponds to an incoming state plus a reflected state on one boundary and an outgoing state on the opposite boundary. To be specific, we consider an incoming state from the left ($K_\perp=-\infty$) in the remainder of this section.

$$\mathbf{\Phi}(K_\perp) = \sum_{\substack{\lambda_i<0,\text{real}\\ \mathrm{Im}\lambda_i<0}} I^i \ \mathbf{\Phi}^{\lambda_i}(K_\perp) + \sum_{\substack{\lambda_i>0,\text{real}\\ \mathrm{Im}\lambda_i>0}} r^i \ \mathbf{\Phi}^{\lambda_i}(K_\perp) \quad \text{for } K_\perp\to-\infty, \tag{18}$$

$$\mathbf{\Phi}(K_\perp) = \sum_{\substack{\lambda_i<0,\text{real}\\ \mathrm{Im}\lambda_i<0}} t^i \ \mathbf{\Phi}^{\lambda_i}(K_\perp) \quad \text{for } K_\perp\to\infty. \tag{19}$$

The first sum in Eq. (18) runs over all incoming propagating states ($\lambda_i<0$, real) and over all states that decay to the right ($\mathrm{Im}\lambda_i<0$). The other sums are defined analogously. The unit vector $\boldsymbol{I}$ with coefficients I^i defines the incoming state. Correspondingly, $\boldsymbol{r}$ and $\boldsymbol{t}$ are the reflected and transmitted amplitudes that have to be determined by Eq. (15). Note that $\mathbf{\Phi}(K_\perp)$ is a vector of dimension equal to the number of Landau level pairs taken into account.

This scattering problem can be solved efficiently by generalizing an approach developed by Fernando and Frensley[28] and Ting *et al.*[29] To this end, we discretize Eq. (15) with respect to $K_\perp$ on an equidistant mesh of step size $\Delta \ll \ell^{-1}$ and consider a finite interval $(-N\Delta, N\Delta)$ where $N \gg 1$. On this mesh, we denote the wave function by $\mathbf{\Phi}_j$, $j=-N,\ldots,N$. The first and second derivatives in Eq. (15) are represented by finite differences involving two and three grid points, respectively. On the left and right boundaries, we can write Eqs. (18), (19) in the form,

$$\begin{pmatrix} \mathbf{\Phi}_{-N} \\ \mathbf{\Phi}_{-N+1} \end{pmatrix} = \boldsymbol{D}\begin{pmatrix} \boldsymbol{I} \\ \boldsymbol{r} \end{pmatrix} = \begin{pmatrix} \boldsymbol{D}_{11} & \boldsymbol{D}_{12} \\ \boldsymbol{D}_{21} & \boldsymbol{D}_{22} \end{pmatrix}\begin{pmatrix} \boldsymbol{I} \\ \boldsymbol{r} \end{pmatrix},$$

$$\begin{pmatrix} \mathbf{\Phi}_{N-1} \\ \mathbf{\Phi}_{N} \end{pmatrix} = \boldsymbol{D}\begin{pmatrix} \boldsymbol{t} \\ \mathbf{0} \end{pmatrix}, \tag{20}$$

were we have introduced the matrix $\boldsymbol{D}$. Using Eqs. (20) and (15), one can eliminate $\boldsymbol{r}$ and $\boldsymbol{t}$ and obtain all wave function coefficients $\mathbf{\Phi}_j$ from the system of linear equations

$$\begin{pmatrix} \mathbf{1} & -\boldsymbol{D}_{12}\boldsymbol{D}_{22}^{-1} & \mathbf{0} & \cdots & \cdots & \cdots & \mathbf{0} \\ \boldsymbol{F} & \boldsymbol{G}_{-N+1} & \boldsymbol{F}^* & \mathbf{0} & \cdots & \cdots & \mathbf{0} \\ \mathbf{0} & \boldsymbol{F} & \boldsymbol{G}_{-N+2} & \boldsymbol{F}^* & \mathbf{0} & \cdots & \mathbf{0} \\ \vdots & & \ddots & \ddots & \ddots & \vdots & \\ \mathbf{0} & \cdots & \cdots & \mathbf{0} & \boldsymbol{F} & \boldsymbol{G}_{N-1} & \boldsymbol{F}^* \\ \mathbf{0} & \cdots & \cdots & \cdots & \mathbf{0} & -\boldsymbol{D}_{21}\boldsymbol{D}_{11}^{-1} & \mathbf{1} \end{pmatrix} \cdot \begin{pmatrix} \mathbf{\Phi}_{-N} \\ \mathbf{\Phi}_{-N+1} \\ \mathbf{\Phi}_{-N+2} \\ \vdots \\ \mathbf{\Phi}_{N-1} \\ \mathbf{\Phi}_{N} \end{pmatrix} = \begin{pmatrix} \boldsymbol{M} \\ \mathbf{0} \\ \mathbf{0} \\ \vdots \\ \mathbf{0} \\ \mathbf{0} \end{pmatrix}, \tag{21}$$

where

$$\boldsymbol{F}=\frac{-1}{\Delta^2\ell^4}\boldsymbol{A}+\frac{i}{2\Delta\ell^2}\boldsymbol{B},$$

$$\boldsymbol{G}_j=\frac{2}{\Delta^2\ell^4}\boldsymbol{A}+\boldsymbol{C}_j-E\ \ \mathbf{1}, \tag{22}$$

$$\boldsymbol{M}=(\boldsymbol{D}_{11}-\boldsymbol{D}_{12}\boldsymbol{D}_{22}^{-1}\boldsymbol{D}_{21})\boldsymbol{I}.$$

The matrix on the left-hand side of Eq. (21) is band diagonal. This equation can possess two types of solutions, namely, propagating ones and bound states. The former are obtained by all possible right-hand sides of Eq. (21) with unit vectors $\boldsymbol{I}$ that correspond to left incoming propagating states (i.e., with λ real and positive). The bound states, on the other hand, are the nontrivial solutions of the homogeneous system of equations obtained by setting $\boldsymbol{I}=\mathbf{0}$. This corresponds to the boundary condition of decaying wave functions for large $|K_\perp|$. The energies where the band matrix is singular determine the bound magnetoexcitons.

As will be explained in Sec. IV, there are bound state solutions $\boldsymbol{\Phi}$ only for energies $E<I_0$. In this regime, all eigenvalues λ are complex. In the opposite energy regime $E>I_0$, the number of solutions $\boldsymbol{\Phi}$ equals the number of real and positive eigenvalues λ. Indeed, one obtains the more real eigenvalues λ the higher the energy E.

III. OPTICAL ABSORPTION

In this section, we calculate the magnetoexcitonic absorption spectrum and present concrete results for GaAs quantum wires. The dipole matrix element for the optical absorption of excitons in the envelope function approximation is given by[30]

$$d=d_{cv}\int d\mathbf{r}\ \Psi(\mathbf{r},\mathbf{r}), \tag{23}$$

where d_{cv} is the interband dipole matrix element between the Bloch valence and conduction band edge states and $\Psi(\mathbf{r}_e,\mathbf{r}_h)$ is the exciton envelope function of Eq. (3). Using Eqs. (2)–(4), one can easily see that only the components $\boldsymbol{\Phi}_{nm}(K_\perp)$ with $n=m$ at $K_\perp=0$ of the coupled channel solutions contribute to the dipole moment. Given the dipole matrix elements, the absorption coefficient at energy E (measured with respect to the effective two-dimensional energy gap $E_{\rm gap}$) is given by

$$\alpha(E)\propto\sum_\nu\left|\sum_n\ \Phi_{nn,\nu}(0)\right|^2\delta(E-E_\nu). \tag{24}$$

The index ν runs over all solutions of the coupled channel equations (13) with energy E_ν, including both the discrete bound states as well as the continuum of scattering states.

The absorption coefficient related to the bound states can be calculated directly from the normalized bound state solutions obtained from the homogeneous version of Eq. (21). The contribution due to the scattering states can be obtained as follows. For given energy $E>I_0$, there are as many scattering states as there are real eigenvalues λ_i that determine the incoming vector $\boldsymbol{I}$ in Eq. (18). Therefore, we can label the propagating scattering states $\boldsymbol{\Phi}(K_\perp)$ by the real eigenvalues λ_i. Each of these eigenvalues defines a continuous branch $\lambda_i(E)$ or, conversely, $E_i(\lambda)$. The sum over all propagating solutions in Eq. (24) corresponds to an integral over the eigenvalues λ and a sum over the different branches (labeled by the index i). In order to evaluate this integral, we use the relation $\delta[E-E_i(\lambda)]=\delta[\lambda_i(E)-\lambda]/|dE_i(\lambda)/d\lambda|$. The density of states factor in this expression can be explicitly evaluated in terms of the solutions of Eq. (17). Since this equation is linear in energy and contains only Hermitian matrices, one can invoke the Feynman-Hellman theorem to obtain

$$\frac{dE_i}{d\lambda}=\boldsymbol{c}^{\lambda_i T}[2\lambda_i\boldsymbol{A}+\boldsymbol{B}]\boldsymbol{c}^{\lambda_i}. \tag{25}$$

Finally, the contribution of the unbound states to the absorption coefficient can be written as

$$\alpha(E)\propto\sum_{\lambda_i>0,\rm real}\frac{2}{|dE_i(\lambda)/d\lambda|}\left|\sum_n\ \Phi_{nn,\lambda_i}(0)\right|^2. \tag{26}$$

The factor of 2 takes into account that the left and right propagating solutions contribute equally to the absorption.

We have calculated this expression for GaAs wires, using the bulk[31] Luttinger parameters $\gamma_1=6.85/m_0$, $\gamma_2=2.10/m_0$, the effective electron mass $m_e=0.067m_0$, and dielectric constant $\epsilon=12.5$. For a magnetic field of $B=10.7$ T, we have considered three different wire widths of $L=L_p=130$ Å, 110 Å, and 100 Å to characterize the confining potentials. The energy unit is effective Rydberg, $R=\mu e^4/2\epsilon^2$, which amounts to $R=3.6$ meV in GaAs. The numerical solution of Eq. (21) was obtained in a basis of ten Landau level pairs and a step size of $\Delta=1/15\ell$, and with 2000 grid points for the $K_\perp$ discretization. Typical results are shown in Fig. 2. The most noticeable feature in these spectra is the occurrence of bound states as well as continuum states with Fano resonances and the suppression of the 1D singularity at the absorption edge that one finds for noninteracting particles.

IV. DISCUSSION

A. Single-channel equations

In order to understand and analyze these structures of the optical spectra, we first approximate Eq. (13) by neglecting all coupling terms between different channels. The resulting single-channel equations greatly facilitate the classification of the general multi-channel solutions. The former read

$$-\frac{1}{2\mu_{\rm eff}}\frac{d^2\Phi_{nm}(K_\perp)}{d(K_\perp\ell^2)^2}+\frac{e^2}{2\ell\epsilon}U_{nm,nm}(K_\perp\ell)\Phi_{nm}(K_\perp)=(E-I_{nm})\Phi_{nm}(K_\perp). \tag{27}$$

As one can see, this is an effective one-dimensional Schrödinger equation in the variable $K_\perp$ that is governed by a kinetic energy term and an effective potential. This potential $e^2U/(2\ell\epsilon)$ is nothing but the *binding energy of the unconfined 2D magnetoexciton* for given $K_\perp$ since the kinetic energy term in Eq. (27) tends to zero in the limit of no confinement. These potentials, or equivalently, the 2D magnetoexciton dispersion relations,[7] are shown in Fig. 3 as

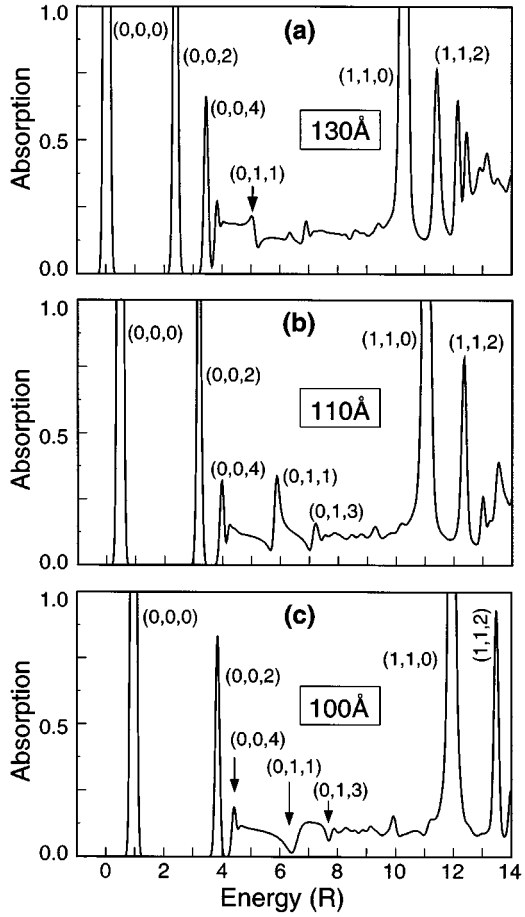

FIG. 2. Predicted optical absorption spectrum of magnetoexcitons in GaAs quantum-well wires of various widths at $B=10.7$ T. The shown spectrum has been convoluted with a Gaussian of width 0.1 R in order to illustrate the relative absorption strengths. The bound states and Fano resonances in the continuum are labeled by (n,m,ν), corresponding to Landau level pairs (n,m) and bound state quantum numbers ν. Energies are given in effective Rydberg (Ry), and the absorption is in arbitrary units. The confining parabolic potential has a width parameter L of (a) 130 Å, (b) 110 Å, and (c) 100 Å.

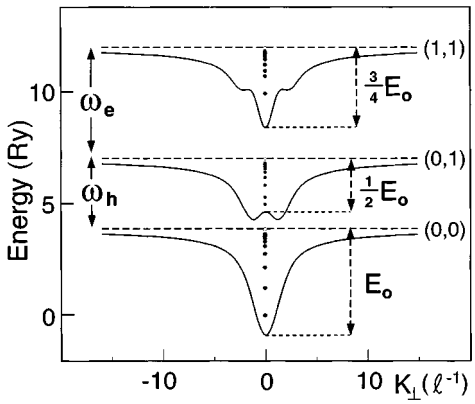

FIG. 3. Energies of two-dimensional magnetoexcitons corresponding to electron and hole Landau level pairs $(n,m)=(0,0)$, $(0,1)$, and $(1,1)$ versus the magnetic momentum $K_\perp$. The ionization energies (dashed lines) are separated by multiples of the respective cyclotron energies, ω_e and ω_h. E_0 is the 2D magnetoexciton binding energy in the ground state. The energy is given in units of effective Rydberg and the momentum is in units of the reciprocal magnetic length. The dots represent the ten lowest solutions of the confined magnetoexciton solutions in the wire within the single-channel approximation. The parameters are the same as in Fig. 2(a).

a function of $K_\perp$ for several channels. We used the same parameters as in Fig. 2. The binding energy of the ground state equals $\sqrt{\pi/2}\ e^2/\epsilon\ell$. The upper limit of the dispersion for channel (n,m) is reached for $K_\perp\to\infty$ and equals I_{nm}, i.e., the sum of the cyclotron energies of the electrons and holes. Therefore, this upper band edge scales linearly with the magnetic field, whereas the bandwidth is determined by the Coulomb term in Eq. (27) and scales with $\sqrt{B}$.

The single-channel equation (27) already reproduces essential confinement effects that are found in the coupled channel equations. Since $U_{nm,nm}(K_\perp\ell)\to-2/K_\perp\ell$ for large $K_\perp$, this effective Schrödinger equation yields an infinite number of bound states below the energy I_{nm} and a continuum of scattering states above it. Thus, I_{nm} plays the role of an ionization energy. The ten lowest bound state energies in each channel are depicted as dots in Fig. 3.

The appearance of a continuum of unbound excitonic states above the bound states is a qualitatively new feature in the 1D case that is also present in the multichannel solutions and should be contrasted with the magnetoexcitonic spectrum in 2D that consists solely of bound states within energy bands of finite width. The formation of a continuum of unbound excitons can be understood qualitatively in two ways. First, let us invoke a simple classical argument. Assume that the electron and hole are optically generated at some position $x_\perp^e\approx x_\perp^h$. They experience a force due to the wire potential that pushes them towards the minimum, $x_\perp^p\to 0$, and leads to a corresponding velocity $v_\perp$. As a consequence, the particles feel a Lorentz force $\pm e(v_\perp\times B)$ that accelerates them in *opposite* directions along the wire. Thus, the particles feel a force that tends to separate the electron and hole.

Second, we would like to elucidate the character of the continuum states by showing that the higher the energy of an unbound electron-hole pair, the farther away it lies from the wire minimum. Let us consider an unbound state above the ionization threshold I_{nm}. The higher the energy, the more the eigenstate will resemble a plane-wave $\exp[iQ(K_\perp\ell^2)]$ with Q representing a continuous parameter, as one can see from Eq. (27). Equation (4) shows that the conjugate variable of $(K_\perp\ell^2)$ is the momentum $k_\parallel$ which implies $k_\parallel^e=-Q$, $k_\parallel^h=Q$. Now, $k_\parallel\ell^2$ determines the mean electron and hole position in $x_\perp$ direction, $\langle x_\perp^e\rangle=\langle x_\perp^h\rangle=Q\ell^2$ as follows from Eq. (2). Consequently, the higher the momentum Q, the more the electron and hole will be pushed up the same side of the confining potential which leads to a continuous increase in the energy of this electron-hole pair. In a 2D situation with no confinement, on the other hand, a shift of the center of mass of the exciton in the plane does not cost any energy.

We note that for finite magnetic fields but zero Coulomb interaction, the single-particle states in a wire potential also form a continuum but no bound states are formed in this case.[17] In the unconfined 2D limit, on the other hand, the eigenstates are dispersionless but nevertheless unbound.

B. Lowest bound states for weak confinement

For weak confining potentials and high fields, $\Omega \ll \omega_c$, we have been able to find analytic solutions of the single-channel equation (27) that further elucidate the physics of 1D magnetoexcitons. Let us consider the lower bound states in channel (n,n) which are characterized by the same Landau level numbers for the electron and the hole. These states feel a potential U exhibiting a minimum at $K_\perp = 0$ as can be seen from Fig. 3. For weak confinement, we can therefore use a harmonic approximation for this potential. In this case, Eq. (27) becomes a harmonic oscillator equation that can be solved analytically. Its eigenvalues are given by

$$E_{nn,\nu} = I_{nn} - \frac{e^2}{2\ell\epsilon}\sqrt{2}\frac{\Gamma(n+1/2)}{\Gamma(n+1)}\,{}_3F_2\left(-n,\frac{1}{2},\frac{1}{2};1,\frac{1}{2}-n;1\right) + \Omega\left(\frac{2R}{\omega_c}\right)^{1/4}\left[\frac{-\sqrt{2}}{8}\frac{\Gamma(n-1/2)}{\Gamma(n+1)} \times {}_3F_2\left(-n,\frac{3}{2},\frac{3}{2};1,\frac{3}{2}-n;1\right)\right]^{1/2}\left(\nu+\frac{1}{2}\right), \qquad (28)$$

where $\nu = 0,1,\ldots$ is the quantum number of the harmonic oscillator that represents the motion of the electron-hole center of mass in the $x_\perp$ direction. The expansion coefficients in the potential $U(K_\perp \ell)$ with respect to $K_\perp$ have been expressed in terms of the generalized hypergeometric functions ${}_3F_2$ that are simple polynomials.

The three terms in Eq. (28) have different orders of magnitude. The first term (the ionization energy I_{nn}) is the largest one and reflects the Landau quantization of the electron and hole. It depends linearly on B. The second term is the Coulomb e-h interaction energy and gives the binding energy of the 2D magnetoexciton. This term is proportional to $\sqrt{B}$. The smallest term is the third one that originates in the quantization of the center-of-mass motion of the 2D magnetoexciton due to the lateral confinement.[7,16] It determines the fine structure of the spectrum and gives the energy separation between the bound states within a channel. It is proportional to $B^{-1/4}$. This term shows that the lateral confinement tends to *reduce* the magnetoexciton ground-state binding energy. This is somewhat surprising since one might expect the confinement to enhance the Coulomb attraction between electron and hole. There is no enhancement, however, since the excitonic wave function gets not only contracted along the $x_\perp$ direction (which would increase the binding energy) but predominantly *elongated* along the $x_\parallel$ direction. This elongation of the e-h wave function leads to a net *reduction* of the Coulomb attraction between electron and hole.

This reduction can be further elucidated by looking at the expectation value of the distance between electron and hole in the ground state. In the harmonic approximation, the ground-state wave function of Eq. (27) is given by $\Phi_{00,0}(K_\perp) \propto \exp[-(K_\perp \ell/\xi)^2]$, where

$$\langle (x_\parallel^e - x_\parallel^h)^2 \rangle = (1+\xi^2/2)\ \ell^2,$$

$$\xi^2 = \frac{2}{(2\pi)^{1/4}}\frac{\Omega}{R}\left(\frac{\omega_c}{2R}\right)^{3/4}. \qquad (29)$$

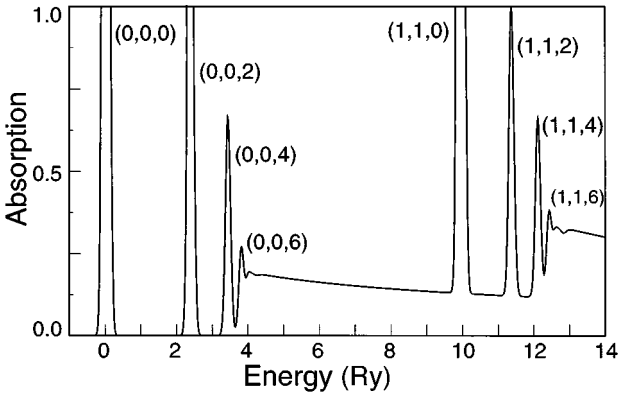

FIG. 4. Optical absorption spectrum of 1D magnetoexcitons. Same as Fig. 2(a), but within the single-channel approximation.

This equation shows quantitatively that a stronger confinement potential indeed elongates the excitonic wave function along the wire axis. We note that $\langle (x_\perp^e - x_\perp^h)^2 \rangle = \ell^2$ is independent of the confinement in the single-channel approximation.

C. Optical absorption spectra

We now discuss the magnetoexciton absorption spectrum. We focus on the single-channel solutions first and consider the effects of channel coupling afterwards. It has already been pointed out that only channels with $n=m$ contribute to the optical absorption. In the single-channel approximation, this implies that the optical spectra can be strictly decomposed into contributions arising from individual channels.

In Fig. 4, we show the absorption spectrum in the single-channel approximation, employing the same parameters as in Fig. 2(a). In the energy range shown, only bound and continuum states of the channels (0,0) and (1,1) appear and have been superimposed in the figure. We have labeled the bound states in each channel by a consecutive index ν, thus characterizing them altogether by quantum numbers (n,n,ν). Since the potential U in the single-channel equation is an even function of $K_\perp$, the bound states possess alternating parity. Only even states contribute to the absorption spectrum, however, as one can deduce from Eq. (24). For this reason, all bound states that are contained in Fig. 4 have even indices ν.

In addition to the bound states, there are unbound single-channel states above the ionization energy I_{nn}. The suppression of the inverse square-root singularity at the ionization threshold is apparent from Fig. 4 and represents another qualitative effect of the Coulomb interaction. One can define a so-called Sommerfeld factor[30] $S(E)$ that is given by the ratio of the absorption coefficient with and without Coulomb interaction. By solving Eq. (27) in the semiclassical approximation,[32] we were able to derive the following simple analytical expression for the Sommerfeld factor of channel (n,n):

$$S(E) = \sqrt{\frac{E - I_{nn}}{E - I_{nn} + (e^2/2\ell\epsilon)\ |U_{nn,nn}(0)|}}\ . \qquad (30)$$

This gives $S(E) < 1$ which is characteristic of 1D systems,[18] and in contrast to the 2D and 3D case where $S(E)$ is gener-

ally larger than one.[33,34] We would like to point out that the suppression of the absorption edge singularity as predicted by the present theory is an intrinsic effect and not caused by lifetime broadening effects that will tend to further smear out the absorption edge.

There is a qualitative difference between the present 1D situation and the case of 2D magnetoexcitons. In the latter case, the momentum $K_\perp$ is a good quantum number in addition to $K_\parallel$. Consequently, only the 2D magnetoexciton states (n,n) at $K_\perp = K_\parallel = 0$ (see Fig. 3) are optically active, leading to a purely discrete absorption spectrum.[11]

Now we discuss the influence of the channel coupling terms in Eq. (13) on the absorption. As is evident from Fig. 2, this coupling induces Fano resonances[4,32] that are caused by the interaction between the bound states of the higher lying channels with energetically degenerate continuum states associated with lower channels.

The prominent structures in the spectra of 1D magnetoexcitons in Fig. 2 can easily be identified in terms of their single-channel quantum numbers (n,m,ν). Only the even bound and quasibound states of the channels (n,n) are optically active and appear in the absorption spectrum. Therefore, they are labeled by even quantum numbers ν. The pronounced Fano resonances in this figure, on the other hand, result from the interaction of the continuum of the (0,0) channel with the quasibound states of the optically inactive channel (0,1). One can deduce from Eqs. (13) and (8) that the coupling operator is an odd function in $K_\perp$, and therefore only odd bound states of channel (0,1) couple to the optically active even scattering states of channel (0,0). Therefore, these resonances can be labeled by the odd quantum numbers associated with these quasibound states.

With increasing confinement the Fano resonances become broader, as one can see in Fig. 2(b). For an even stronger confinement, the absorption gets strongly suppressed at the Fano resonances. This leads to the dip-shaped ''window resonances,''[32] that are depicted in Fig. 2(c).

For 2D magnetoexcitons, there are no unbound states and consequently no Fano resonances. The coupling between channels only shifts the discrete absorption lines in energy.[11]

V. CONCLUSIONS

In this paper, a detailed study of the electronic properties and optical absorption of magnetoexcitons in a quantum-well wire has been presented. Starting from 2D magnetoexcitons, the effects of confinement of electrons and holes by a one-dimensional parabolic potential have been studied.

In contrast to the two-dimensional situation where all magnetoexciton states are bound,[7] we have shown that 1D magnetoexcitons possess a hydrogenic spectrum with an infinite number of bound states and a continuum of scattering states at higher energies. In several limiting cases, analytical results for these states have been derived.

The appearance of unbound states has been shown to lead to another peculiar effect that is characteristic of 1D systems: the Coulomb interaction causes the optical magnetoexcitonic absorption spectrum of the unbound states to be a smooth function of energy, that is characterized by a Sommerfeld factor *smaller* than unity. An analytic expression for the Sommerfeld factor of 1D magnetoexcitons has been derived.

We have presented a method for calculating the wave functions of bound and unbound magnetoexcitons by using an efficient scattering approach, which allows a fine resolution of the resonance structures in the absorption spectrum. We have also shown that the 1D magnetoexciton spectrum can be classified by the Landau quantum numbers (n,m) of 2D magnetoexcitons and by quantum numbers that label the single-channel bound states. The coupling between bound and continuum states associated with different channels leads to the formation of pronounced Fano resonances associated with optically forbidden quasibound state transitions.

ACKNOWLEDGMENTS

Financial support by the Deutsche Forschungsgemeinschaft (SFB 348), Bayerische Forschungsverbund (FOROPTO) and Volkswagenstiftung is gratefully acknowledged.

APPENDIX: COULOMB MATRIX ELEMENTS

In Eq. (3), we have represented the excitonic wave function in the basis of 2D magnetoexcitons in the Landau gauge. This basis is characterized by e-h–Landau level pairs (n,m) and magnetic momentum $\mathbf{K}=(K_\perp,K_\parallel=0)$. We wish to calculate the two-dimensional Coulomb interaction in this basis. Its matrix elements are defined in Eq. (7). Here, we discuss some intermediate steps that lead to Eq. (8). By inserting the basis functions, Eqs. (4) and (2), into Eq. (7), one obtains

$$
\begin{aligned}
U_{n'm',nm}(K_\perp \ell) = {} & \frac{(-1)^{n'-n}}{\pi}\sqrt{\frac{n!\ m'!}{n'!\ m!}}\int_0^\infty dq \\
& \times \int_0^{2\pi} d\varphi\ e^{i\ \varphi\ N}\left(\frac{q}{\sqrt{2}}\right)^N e^{-(1/2)q^2} \\
& \times \exp\{i\ \ q\ \ K\ell\ \ \cos[\pi/2+\varphi]\} \\
& \times L_n^{n'-n}\left(\frac{q^2}{2}\right) L_{m'}^{m-m'}\left(\frac{q^2}{2}\right) \\
= {} & 2\ \ (-1)^{n'-n}\ \ i^N\ \ \sqrt{\frac{n!\ m'!}{n'!\ m!}}\int_0^\infty dq \\
& \times J_N(K\ell\ \ q)\left(\frac{q}{\sqrt{2}}\right)^N e^{-(1/2)q^2} \\
& \times L_n^{n'-n}\left(\frac{q^2}{2}\right) L_{m'}^{m-m'}\left(\frac{q^2}{2}\right), \qquad \text{(A1)}
\end{aligned}
$$

where $N=n'-n-m'+m$. The angular integration in Eq. (A1) yields the Bessel functions J_N of order N, and the subsequent integration over q leads to the degenerate hypergeometric functions of Eq. (8). For large values of $K_\perp$, the matrix elements are of the order $O(|K_\perp|^{-(|N|+1)})$, whereas $U_{n'm',nm}=O(|K_\perp|^{|N|})$ for $|K_\perp|\ell \ll 1$. A generalization to nonvanishing $K_\parallel$ is straightforward.

[1] R. J. Elliot and R. Loudon, J. Phys. Chem. Solids **15**, 196 (1960).
[2] H. Hasegawa and R. E. Howard, J. Phys. Chem. Solids **21**, 179 (1961).
[3] L. P. Gor'kov and I. E. Dzyaloshinskĭ, Zh. Éksp. Teor. Fiz. **53**, 1167 (1967) [Sov. Phys. JETP **26**, 449 (1967)].
[4] U. Fano, Phys. Rev. **124**, 1866 (1961).
[5] S. Glutsch, U. Siegner, M.-A. Mycek, and D. S. Chemla, Phys. Rev. B **50**, 17 009 (1994).
[6] Uwe Siegner, Mary-Ann Mycek, Stephan Glutsch, and Daniel S. Chemla, Phys. Rev. B **51**, 4953 (1995).
[7] I. V. Lerner and Yu. E. Lozovik, Zh. Éksp. Teor. Fiz. **78**, 1167 (1980) [Sov. Phys. JETP **51**, 588 (1980)].
[8] Okikazu Akimoto and Hiroshi Hasegawa, J. Phys. Soc. Jpn. **22**, 181 (1967).
[9] A. H. MacDonald and D. S. Ritchie, Phys. Rev. B **33**, 8336 (1986); in this paper only shallow impurity energy levels in 2D are considered, but the result is also applicable to the case of 2D magnetoexcitons with zero center-of-mass momentum.
[10] S. Schmitt-Rink, J. B. Stark, W. H. Knox, D. S. Chemla, and W. Schäfer, Appl. Phys. A **53**, 491 (1991).
[11] Charles Stafford and Stefan Schmitt-Rink, Phys. Rev. B **41**, 10 000 (1990).
[12] Takuji Tanaka, Yasuhiko Arakawa, and Gerrit W. E. Bauer, Phys. Rev. B **50**, 7719 (1994).
[13] A. Balandin and S. Bandyopadhyay, Phys. Rev. B **52**, 8312 (1995).
[14] Gang Li, Spiros V. Branis, and K. K. Bajaj, J. Appl. Phys. **77**, 1097 (1995).
[15] V. Halonen, T. Chakraborty, and P. Pietiläinen, Phys. Rev. B **45**, 5980 (1992).
[16] A. B. Dzyubenko and A. Yu. Sivachenko, J. Phys. (France) IV **3**, 381 (1993).
[17] W. Tan, J. C. Inkson, and G. P. Srivastava, Semicond. Sci. Technol. **9**, 1305 (1994).
[18] Tetsuo Ogawa and Toshihide Takagahara, Phys. Rev. B **44**, 8138 (1991).
[19] S. Glutsch and F. Bechstedt, Phys. Rev. B **47**, 4315 (1993).
[20] S. Glutsch, D. S. Chemla, and F. Bechstedt, Phys. Rev. B **51**, 16 885 (1995).
[21] M. Altarelli and N. O. Lipari, Phys. Rev. B **9**, 1733 (1974).
[22] Ronald L. Greene and K. K. Bajaj, Phys. Rev. B **31**, 6498 (1985).
[23] A. B. Dzyubenko and Yu. E. Lozovik, Fiz. Tverd. Tela (Leningrad) **25**, 1519 (1983) [Sov. Phys. Solid State **25**, 874 (1983)]; **26**, 1540 (1984) [**26**, 938 (1984)].
[24] C. Kallin and B. I. Halperin, Phys. Rev. B **30**, 5655 (1984).
[25] I. S. Gradshteyn and I. M. Ryzhik, *Table of Integrals, Series, and Products* (Academic, San Diego, 1980).
[26] M. L. Glasser and Norman J. Morgenstern Horing, Phys. Rev. B **31**, 4603 (1985).
[27] W. H. Press, B. P. Flannery, S. A. Teukolsky, and W. T. Vetterling, *Numerical Recipes: The Art of Scientific Computing* (Cambridge University Press, Cambridge, 1992).
[28] C. L. Fernando and W. R. Frensley, J. Appl. Phys. **76**, 2881 (1994).
[29] D. Z.-Y. Ting, E. T. Yu, and T. C. Mc-Gill, Phys. Rev. B **45**, 3583 (1992).
[30] H. Haug and St. W. Koch, *Quantum Theory of the Optical and Electronic Properties of Semiconductors* (World Scientific, Singapore, 1993).
[31] *Physics of Group IV Elements and III-V Compounds*, edited by O. Madelung, H. Weiss, and M. Schulz, Landolt-Börnstein, New Series, Group III, Vol. 17, Pt. a (Springer, Heidelberg, 1982), Sec. 2.
[32] H. Friedrich, *Theoretical Atomic Physics* (Springer, New York, 1991).
[33] R. J. Elliott, Phys. Rev. **108**, 1384 (1957).
[34] M. Shinada and S. Sugano, J. Phys. Soc. Jpn. **21**, 1936 (1966).